How disorder affects topological surface states in the limit of ultrathin Bi_2Se_3 films ?

Kenan Song[1], Roberto Robles[1], David Soriano[1], Pablo Ordejon[1] and Stephan Roche[1,2]

[1]*Catalan Institute of Nanoscience and Nanotechnology (ICN2),*

CSIC and The Barcelona Institute of Science and Technology,

Campus UAB, Bellaterra, 08193 Barcelona, Spain

[2]*ICREA, Institució Catalana de Recerca i Estudis Avançats, 08070 Barcelona, Spain*

(Dated: June 13, 2016)

Abstract

We present a first-principles study of electronic properties of ultrathin films of topological insulators and scrutinize the role of disorder on the robustness of topological surface states, which can be analysed through their spin textures. The presence of twin grain boundaries is found to increase the bandgap of the film, while preserving the spin texture of states in first conduction and valence bands. Differently, partial hydrogenation of one surface not only results in some self-doping effect, but also provokes some alteration of the spin texture symmetry of the electronic states. The formation of a new Dirac cone at M-point of the Brillouin zone of the hydrogenated surface, together with a modified spin texture characteristics are consistent with a dominant Dresselhaus spin-orbit interaction type, more usually observed in 3D materials. Our findings indicate that defects can either be detrimental or beneficial for exploring spin transport of surface states in the limit of ultrathin films of topological insulators, which maximizes surface over bulk phenomena.

INTRODUCTION

Topological insulators (TIs) represent a new state of Condensed Matter with unique electronic structure, insulating in the bulk but conducting at their boundaries with a Dirac cone shape at low energies [1–3]. The corresponding boundary states are protected by time reversal symmetry with a spin-momentum locking character, namely the direction towards which the carriers are travelling determines univocally the direction of the spin, thus resulting in intrinsic spin currents and unprecedented opportunities for innovative spintronics [3]. Bernevig and Zhang predicted the existence of TIs in strong spin-orbit coupling materials [4, 5], and revealed through the formation of edge channels with quantized conductance, later confirmed experimentally in Cadmium Telluride/Mercury telluride/Cadmium Telluride (CdTe/HgTe/CdTe) quantum wells through transport measurements [6]. Three-dimensional bulk solids of binary compounds involving bismuth were then predicted to also belong to the topological insulators family [7]. The first experimentally realized 3D topological insulator state was reported in bismuth antimonide [8], and shortly after observed in pure antimony, bismuth selenide Bi_2Se_3, bismuth telluride and antimony telluride using ARPES (see Ref.[3]).

However, to date, the 3D topological insulators do not truly insulate [1, 2], and despite some indications of signatures of the exotic surface states in transport measurements, the contribution of defects and bulk transport remains a big hurddle to fully exploit the potential of those materials [9–11]. Additionally, growing large area of high-quality TI-films by MBE remains a true challenge, so minimizing the "bulk" part of the TI is a strategy to preserve larger surface versus bulk transport channels. The symmetry breaking of opposite surfaces of TI (for instance through chemical functionalization or substrate effects [12, 13]) has been further shown to suppress the quantum tunneling between surface states, hence offering the possibility for exploring spin transport at surface of ultrathin TI films. The remaining important question is to quantify the impact of individual defects (twin grain boundaries, vacancies, oxygen defects, ad-atoms, substitutional impurities,...) in such circumstances [14–16].

Here, using first-principles calculations, we investigate the detrimental effect of twin grain boundaries and surface doping in the limit of thin TI films. We study two different types of defects which may affect strongly the electronic structure of low dimensional topological insulators: (1) twin grain boundaries where adjacent QLs become rotated 180° with respect to the other (Figure S1(b)), and (2) surface doping induced by hydrogen adatoms (Figure S1(c)). As a limiting case, we also study how the topological surface states are modified when both defects are present in the same sample (Figure S1(d))

METHODOLOGY

First principles calculations were carried out in the framework of the density-functional theory (DFT) as implemented in the Vienna Ab initio Simulation Package (VASP) [17]. Wave functions were expanded by means of plane-wave basis sets with an energy cutoff of 450 eV. The projector augmented wave (PAW) method was used to describe core electrons [18, 19]. For the exchange-correlation energy we used the generalized gradient approximation (GGA) in the PBE form [20]. We used a 11x11x1 k-point mesh used to sample the Brillouin zone. Missing dispersion forces were included using theTkatchenko-Scheffler method. [21] The lattice structure was relaxed until the forces on each atom were smaller than 10^{-3} eV/Å.

The crystal structure of Bi_2Se_3 is rhombohedral. Bismuth and selenium atoms combine forming quintuple layers that stack together along the (111)-direction by means of van der Waals interactions (see Figure S1(a)). In this work we focus on unit cells containing only three quintuple layers (~ 3 nm), and describe the impact of fully saturated surface atoms and twin boundaries on the electronic band structure as well as on the spin texture of low-energy states. The spin texture is analysed by plotting the expectation value of the spin operators in a properly chosen set of k-points.

RESULTS

Twin grain boundaries in Bi_2Se_3 thin films

Figure S2(a) shows the band structure of a pristine 3QL Bi_2Se_3 slab. Due to the small thickness of the film, a small gap of 36 meV opens at the Fermi level owing to the interaction between surface states at opposite boundaries. Upon a rotation of the bottom layer of the slab by 180° and subsequent geometry relaxation, we do not observe strong variations of the lattice constants within each QL. In contrast, the van der Waals spacing between the middle QL and the bottom one increases from 2.576 Å to 3.589 Å. Figure S2(b) shows however that the twin grain boundary case yields an enhancement of the energy gap up to 194 meV.

Such impact on the electronic band structure is likely related to the fact that the Se layers between the rotated and the original QLs become aligned in x-y plane after the rotation, increasing the Coulomb repulsion. This results in a larger interlayer spacing and the gap enlargement. It is interesting to mention that, despite the large increase of the gap, the spin texture corresponding to the topological surface states

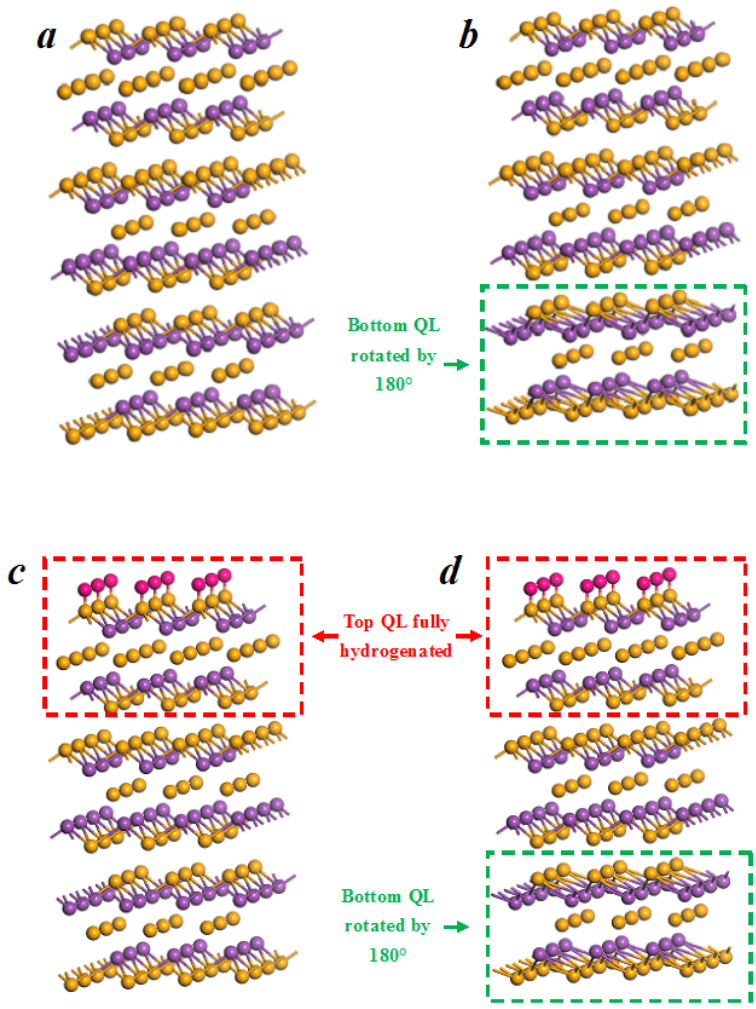

FIG. S1. Model of 3-QLs Bi_2Se_3 slabs used in the calculations. (a) Pristine slab; (b) Slab with the bottom QL rotated by 180°; (c)-(d) Same slabs as in (a)-(b) where the top surface has been fully hydrogenated. Bi, Se and H atoms are represented in purple, orange and magenta, respectively.

is still preserved.

To confirm that the increased gap value is related to the interlayer spacing between the last two QLs, we compute the magnitude of the gap while varying the distance between middle and bottom QLs starting from the relaxed structure. The results are plotted in figure S2(e) and, as expected, they show an increase of the band gap for larger interlayer spacing. The presence of such grain boundaries in the 3 nm ultrathin

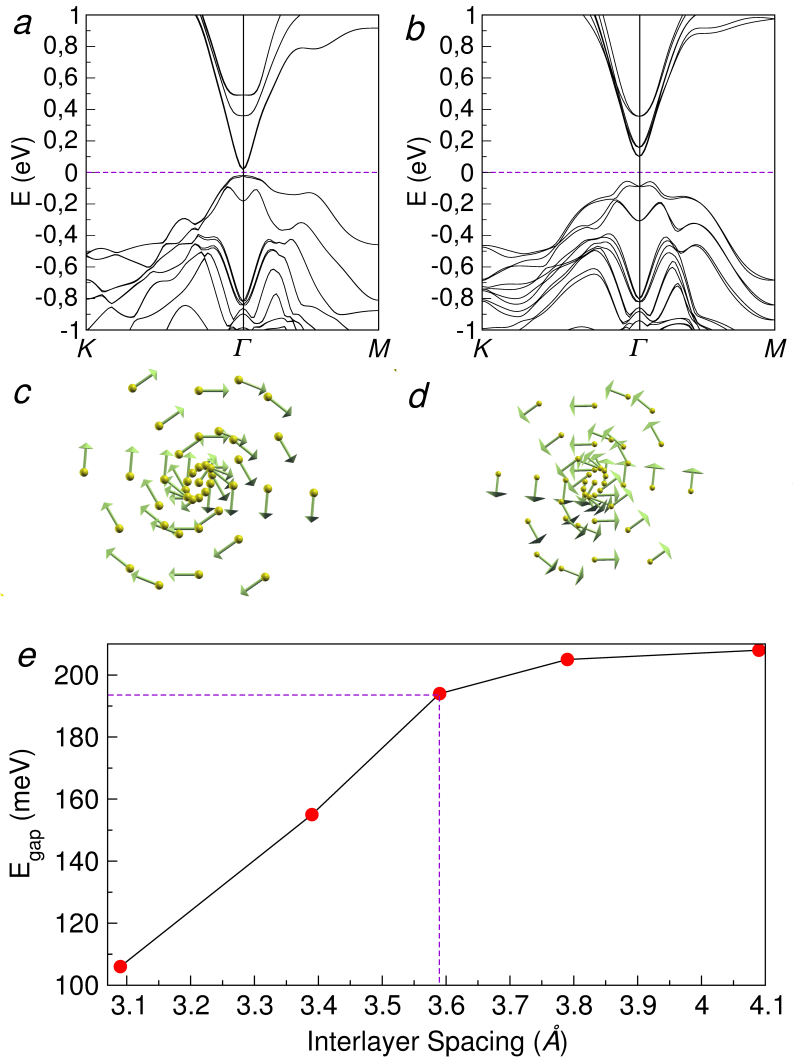

FIG. S2. Bandstructures of 3QL Bi_2Se_3 pristine (a) and with the bottom QL rotated by 180° (b). Spin textures of the topological surface states in absence (d) and in presence (c) of the twin grain boundary. The spin polarization is calculated from the bottom of the conduction band to E = 0.15 eV. (e) Evolution of the band gap while increasing the spacing between the middle and the rotated bottom QLs. The dashed lines show the equilibrium distance.

film also induces a very small energy level splitting due to the breaking of inversion symmetry.

In a similar work by Aramberri *et al* on thicker Bi_2Se_3 films [22], it was shown that twin boundaries induce either n- or p-type self-doping on the surface states (up to 300 meV), depending on the relative orientation of adjacent QLs. Such self-doping stems from spontaneous polarization generated by the dipole moments associated with the lattice defects. However in such study on thicker TI-films, no gap

opening due to the presence of this type of defects was observed. This highlights the importance of reducing the number of defects when producing low dimensional TIs.

Effect of surface doping on Bi_2Se_3 thin films

Another important effect that may appear when ultrathin TI fims are grown or deposited on top of a substrate is surface doping. To mimic this effect, we have fully saturated one of the surfaces of our Bi_2Se_3 slab with hydrogen atoms (see Fig. S1(c)). After full relaxation, the distance between H and Se atoms was found to be 1.52Å. Figure S3 shows the band structures and spin textures of the partially hydrogenated 3QL Bi_2Se_3 slabs projected onto the hydrogen terminated top QL (red circles) and the pristine bottom QL (green circles) while varying the H-Se distance. First, we observe the formation of surface dipoles when the hydrogen atoms start to approach the surface leading to a downward shift of the surface bands at the Γ-point, and also to the formation of Rashba-like states as experimentally observed on potassium doped Bi_2Se_3 samples [23]. Second, and more importantly, the gapless surface states remain metallic after hydrogen absorption. This is mainly driven by the breaking of inversion symmetry which splits the Dirac points at both surfaces reducing surface-to-surface interaction. Meanwhile, the spin texture at the Γ-point corresponding to the undoped topological surface states, reflects the usual in-plane polarisation (see Fig.S3(d)) thus preserving the spin-momentum locking.

As previously observed [12, 24, 25], surface modification of Γ-centered TIs may gives rise to new non-trivial surface states centered at the three M-points of the Brillouin zone (red circles in Fig. S3). The origin of such new surface states seem to be related to the presence of dangling bonds appearing during cleaving process [26] due to the formation of non-stoichiometric surface terminations like Se-Bi-Se or Se-Bi. Here, the new surface or midgap states appear by a simple chemical saturation of the top Se atoms by hydrogen. This case is even more interesting than non-stoichiometric surface terminations since the latter ones are highly reactive and may tend to reconstruct.

A detailed analysis of the atomic orbitals involved on the formation of this new state is shown in Fig. S4, where one plots the band structures of pristine (a,b) and hydrogenated (c,d) slabs projected onto the atomic orbitals of the surface Se (left panel) and Bi (right panel) atoms. After hydrogenation, the bands corresponding to the p_z orbitals of the Se atoms (yellow circles) disappear from the low-energy region due to the hybridization with the $1s$ orbitals of the H atoms. On the other hand, the p_z orbitals of the Bi surface atoms that mainly contribute to the formation of the topological surface states in the pristine

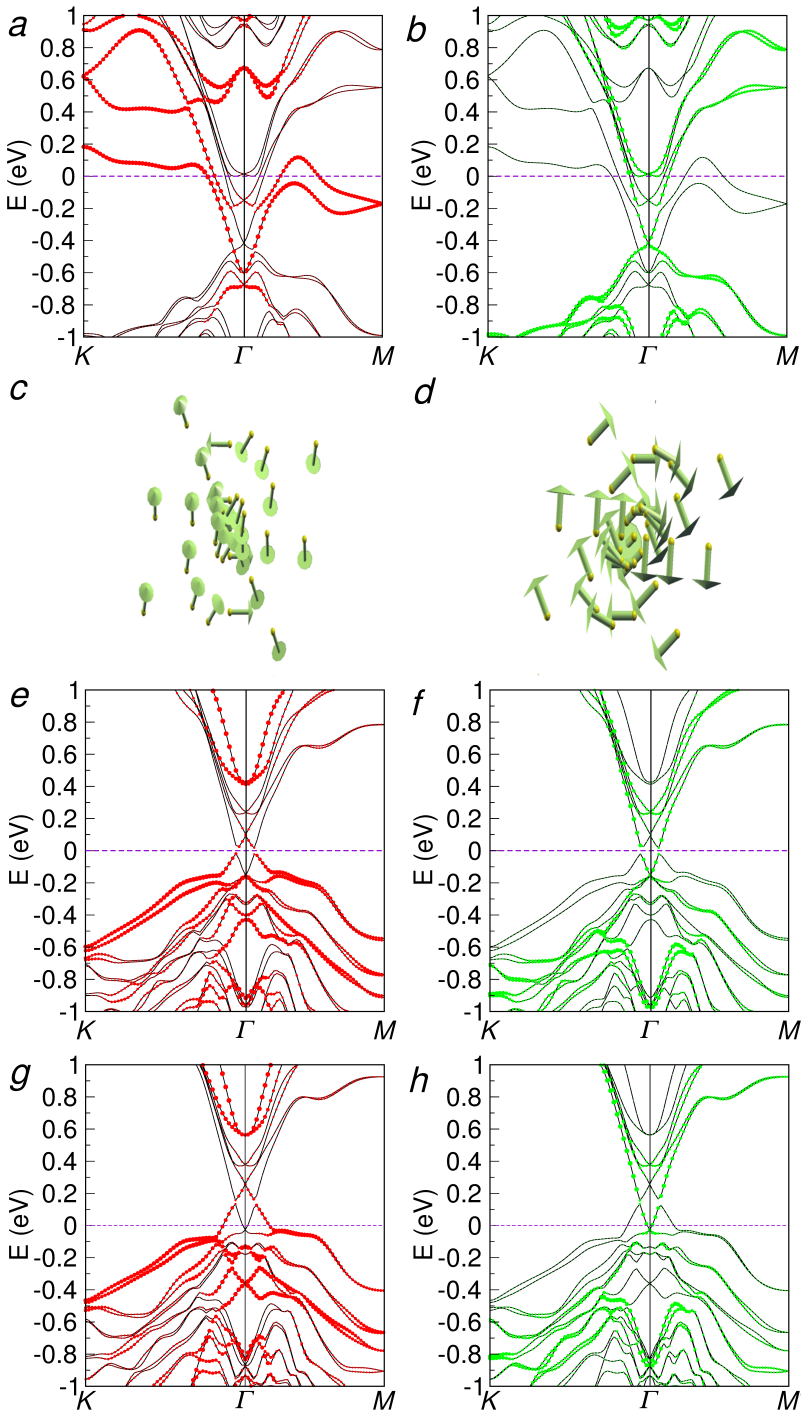

FIG. S3. Top panel shows the band structure of fully relaxed 3QL Bi_2Se_3 slab with top QL hydrogenation (H-Se distance is 1.52Å). Red and green symbols indicate the projection on the top (a) and bottom (b) QLs. Second pannel shows the spin texture at one of the M-points (c) and at the Γ-point (d). Rest of the panels show the band structure of the same system, but for larger H-Se distance: 3.52Å(e)-(f) and 5.52Å(g)-(h).

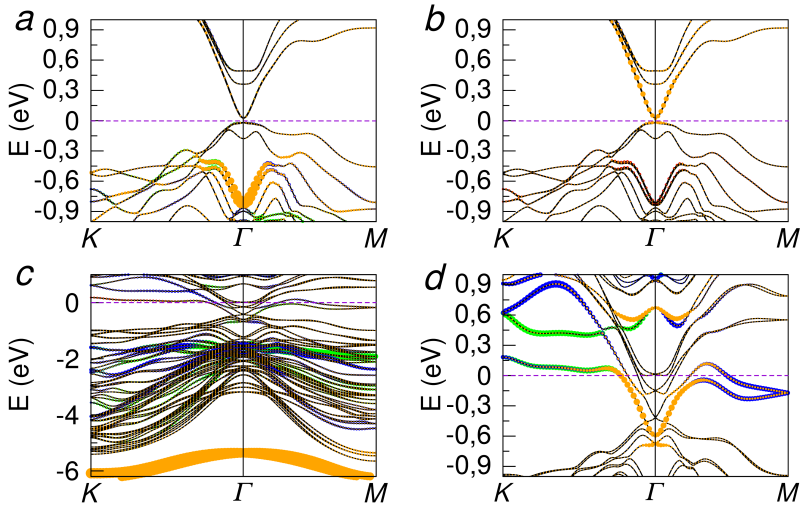

FIG. S4. Atomic orbital projection of the top Se (left panel) and Bi (right panel) atoms on the band structures corresponding to the pristine 3QL Bi_2Se_3 case (a,b) and the hydrogenated case (c,d). The different colours correspond to $1s$ (red), p_x (green), p_y (blue) and p_z (yellow).

case, are still present after the hydrogenation but at lower energy (Fig. S4(b,d)). More interestingly, while typical topological surface states centered at the Γ-point show a strong p_z contribution from the top QL atoms, now the contribution of the p_y orbitals from the Bi atoms of the second layer on the new topological surface states at M is even stronger than the p_z orbital contribution, which manifests the presence of in-plane dangling bonds in the top Bi-Se interface. Also, the spin texture associated with this new Dirac cone shows a spin-momentum locking configuration which resembles that of a Dresselhaus spin-orbit interaction typical of 3D materials, with a strong out-of-plane spin polarisation (Fig.S3(c)).

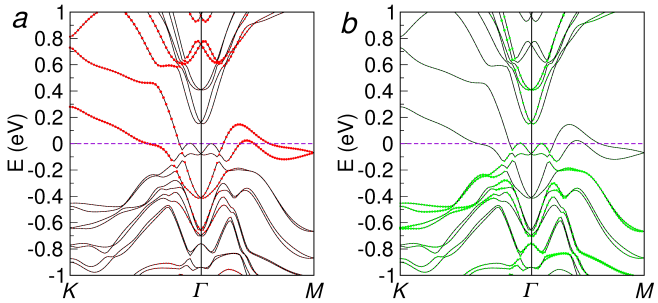

FIG. S5. Band structure of 3QL Bi_2Se_3 with the bottom QL rotated by 180° and the top layer fully hydrogenated. Red and green circles show the projection onto the top and bottom QLs respectively.

Combining twin grain boundaries and surface doping in Bi_2Se_3 thin films

We finally consider the joint contribution of both twin grain boundary and hydrogenation introduced into the 3QLs Bi_2Se_3 film. Se atoms on the top surface are fully saturated by hydrogen atoms while the bottom QL is rotated by 180° (figure S1(d)). Figure S5 shows the resulting band structures at opposite surfaces. Interestingly, the presence of the additional Dirac cone at M-point is insensitive to the presence of the twin grain boundary. It is important to note that the presence of the twin boundary along the (111) direction and the saturation of the top Se atoms give rise to an interesting situation in which electrons may flow easily on the top surface due to the presence of the new surface state band coming from the dangling bonds (red circles), while they cannot do it in the opposite surface due to the appearance of a new gap of the order of 200 meV (green circles).

CONCLUSIONS

In conclusion, we have studied the impact of different defects on the electronic properties of ultrathin films of TIs. Twin grain boundaries are found to enhance the electronic bangap of the film, without changing the symmetry of surface states spin texture, contrary to the case of hydrogen adatoms which modify the spin texture symmetry (similar to Dresselhaus spin-orbit interaction type [12]) of the electronic states and generate a new Dirac cone at M-point at the brillouin zone of the hydrogenated surface. Our results evidence that in the ultrathin limit, the nature of defect crucially impacts on the variability of the spin-dependent features of the electronic spectrum, which is simultaneously a limitation for fine-tune control of surface states in situation of large surface versus bulk ratio, but also suggests interesting directions to explore the spin dynamics of new electronic excitations generated by impurity bands.

ACKNOWLEDGEMENTS

This work has received funding from the Spanish Ministry of Economy and Competitiveness and the European Regional Development Fund (Project No. FIS2015-67767-P (MINECO/FEDER)) and the Severo Ochoa Program (MINECO SEV-2013-0295). The authors also thank the Secretaria de Universidades e Investigación del Departamento de Economía y Conocimiento de la Generalidad de Cataluña.

[1] M. Z. Hasan and C. L. Kane, Rev. Mod. Phys. **82**, 3045 (2010).

[2] X.-L. Qi and S.-C. Zhang, Rev. Mod. Phys. **83**, 1057 (2011).

[3] F. Ortmann, S. Roche, and S. O. Valenzuela, in *Topological Insulators, Fundamentals and Perspectives* (Wiley-VCH Verlag GmbH and Co. KGaA, 2015).

[4] B. A. Bernevig and S.-C. Zhang, Phys. Rev. Lett. **96**, 106802 (2006).

[5] B. A. Bernevig, T. L. Hughes, and S.-C. Zhang, Science **314**, 1757 (2006).

[6] M. König, S. Wiedmann, C. Brüne, A. Roth, H. Buhmann, L. W. Molenkamp, X.-L. Qi, and S.-C. Zhang, Science **318**, 766 (2007).

[7] L. Fu and C. L. Kane, Phys. Rev. B **76**, 045302 (2007).

[8] D. Hsieh, D. Qian, L. Wray, Y. Xia, Y. Hor, R. J. Cava, and M. Z. Hasan, Nature **452**, 970 (2008).

[9] C. Brüne, C. X. Liu, E. G. Novik, E. M. Hankiewicz, H. Buhmann, Y. L. Chen, X. L. Qi, Z. X. Shen, S. C. Zhang, and L. W. Molenkamp, Phys. Rev. Lett. **106**, 126803 (2011).

[10] J. G. Checkelsky, Y. S. Hor, M.-H. Liu, D.-X. Qu, R. J. Cava, and N. P. Ong, Phys. Rev. Lett. **103**, 246601 (2009).

[11] M. V. Costache, I. Neumann, J. F. Sierra, V. Marinova, M. M. Gospodinov, S. Roche, and S. O. Valenzuela, Phys. Rev. Lett. **112**, 086601 (2014).

[12] D. Soriano, F. Ortmann, and S. Roche, Phys. Rev. Lett. **109**, 266805 (2012).

[13] X.-G. Zhu and P. Hofmann, Phys. Rev. B **89**, 125402 (2014).

[14] G. Wang, X.-G. Zhu, Y.-Y. Sun, Y.-Y. Li, T. Zhang, J. Wen, X. Chen, K. He, L.-L. Wang, X.-C. Ma, J.-F. Jia, S. B. Zhang, and Q.-K. Xue, Advanced Materials **23** (2011).

[15] A. Richardella, A. Kandala, J. S. Lee, and N. Samarth, APL Mater. **3** (2015).

[16] C. Kastl, P. Seifert, X. He, K. Wu, Y. Li, and A. Holleitner, 2D Materials **2**, 024012 (2015).

[17] G. Kresse and J. Furthmüller, Computational Materials Science **6**, 15 (1996).

[18] P. E. Blöchl, Physical Review B **50**, 17953 (1994).

[19] G. Kresse and D. Joubert, Physical Review B **59**, 1758 (1999).

[20] J. P. Perdew, K. Burke, and M. Ernzerhof, Phys. Rev. Lett. **77**, 3865 (1996).

[21] A. Tkatchenko and M. Scheffler, Phys. Rev. Lett. **102**, 073005 (2009).

[22] H. Aramberri, J. I. Cerdá, and M. C. Muñoz, Nano Letters **15**, 3840 (2015).

[23] Z.-H. Zhu, G. Levy, B. Ludbrook, C. N. Veenstra, J. A. Rosen, R. Comin, D. Wong, P. Dosanjh, A. Ubaldini, P. Syers, N. P. Butch, J. Paglione, I. S. Elfimov, and A. Damascelli, Phys. Rev. Lett. **107**, 186405 (2011).

[24] G. Bian, X. Wang, Y. Liu, T. Miller, and T.-C. Chiang, Phys. Rev. B **84**, 235414 (2011).

[25] X.-G. Zhu and P. Hofmann, Phys. Rev. B **89**, 125402 (2014).

[26] H. Lin, T. Das, Y. Okada, M. C. Boyer, W. D. Wise, M. Tomasik, B. Zhen, E. W. Hudson, W. Zhou, V. Madhavan, C.-Y. Ren, H. Ikuta, and A. Bansil, Nano Letters **13**, 1915 (2013).